

# **Experimental validation of Advanced Dispersed Fringe Sensing (ADFS) algorithm using Advanced Wavefront sensing and Correction Testbed (AWCT)**

Xu Wang, Fang Shi, Norbert Sigrist, Byoung-Joon Seo, Hong Tang, Siddarayappa Bikkannavar, Scott Basinger, Oliver Lay  
Jet Propulsion Laboratory, California Institute of Technology, Pasadena, CA 91109-8099

## **ABSTRACT**

Large aperture telescope commonly features segment mirrors and a coarse phasing step is needed to bring these individual segments into the fine phasing capture range. Dispersed Fringe Sensing (DFS) is a powerful coarse phasing technique and its alteration is currently being used for JWST. An Advanced Dispersed Fringe Sensing (ADFS) algorithm is recently developed to improve the performance and robustness of previous DFS algorithms with better accuracy and unique solution. The first part of the paper introduces the basic ideas and the essential features of the ADFS algorithm and presents the some algorithm sensitivity study results. The second part of the paper describes the full details of algorithm validation process through the advanced wavefront sensing and correction testbed (AWCT): first, the optimization of the DFS hardware of AWCT to ensure the data accuracy and reliability is illustrated. Then, a few carefully designed algorithm validation experiments are implemented, and the corresponding data analysis results are shown. Finally the fiducial calibration using Range-Gate-Metrology technique is carried out and a <10nm or <1% algorithm accuracy is demonstrated.

**Key words:** Dispersed Fringe Sensing, DFS, JWST, WFSC, GRISM

## **1. INTRODUCTION**

Current large aperture telescope typically features segment mirror for its primary. A coarse phasing step is needed to bring the individual segments into the fine phasing capture range. Dispersed Fringe Sensing (DFS) serves this purpose well. In JPL, F. Shi first developed a suite of Matlab codes to implement the DFS algorithm<sup>1</sup>, and then multiple people (B.King, J. Spechler, and S. Bikkannavar) worked on it to continuously improve its performance. For example, J. Spechler developed an angular DFS (ADFS) where the fringe extraction line is dithered angularly to find the best signal fitting, whose results turns out to be less sensitive to some calibration errors<sup>2</sup>. Built upon these DFS technology developments accumulated over the past few years, a new ADFS algorithm featuring multi-dimensional-scan is recently developed and has been validated successfully using Advanced Wavefront Sensing and Control Testbed (AWCT)<sup>3</sup>. Unlike the previous ADFS where fringe extraction line was dithering only angularly, the new ADFS varies the fringe extraction line in multiple dimensions (both translation and rotation). The extra degree freedom in the dithering domain and the overall averaging effect enable the new ADFS to achieve a unique and accurate solution, which greatly improves the performance and robustness of the algorithm. This document describes some major features of

---

\*xu.wang@jpl.nasa.gov; phone: 818-393-0229; fax: 818-393-4357; <http://www.jpl.nasa.gov>

this ADFS development and its validation results through various experiments done on AWCT.

## 2. IMPROVEMENT OF THE ADFS ALGORITHM

### 2.1 Description of the typical ADFS

ADFS algorithm mainly involves processing a few interferometer images taken with different spectral filters. A typical fringe processing includes essentially 4 process steps: 1)wavelength vector process which calculates the centroids of a few wavelength calibration images (taken with different narrow band filter) to extract the (wave\_cent, wave\_lambda) vector. 2)Fringe Extraction Line (FEL) process which generates an array of wave vectors (xx, yy, wavelength) to cover the full spectral range using the coefficient extracted from the linear fit of the (wave\_cent, wave\_lambda) vector. 3)reference process which figures out the reference signal (ref\_line) along (xx, yy) from the reference image(taken with board band filter). 4)fringe analysis process which is basically a nonlinear least square fit to extract the piston information out of the fringe pattern with the help of the above processed calibration information (xx, yy, wavelength, ref\_line).

Figure 1 shows the major outline/result of the DFS fringe processing: upper left is the wavelength calibration on CCD; upper right is the FEL (yellow dash spots across the fringe); lower left is the reference signal (FEL points along the source spectrum on CCD); lower right is the fringe curve fitting results.

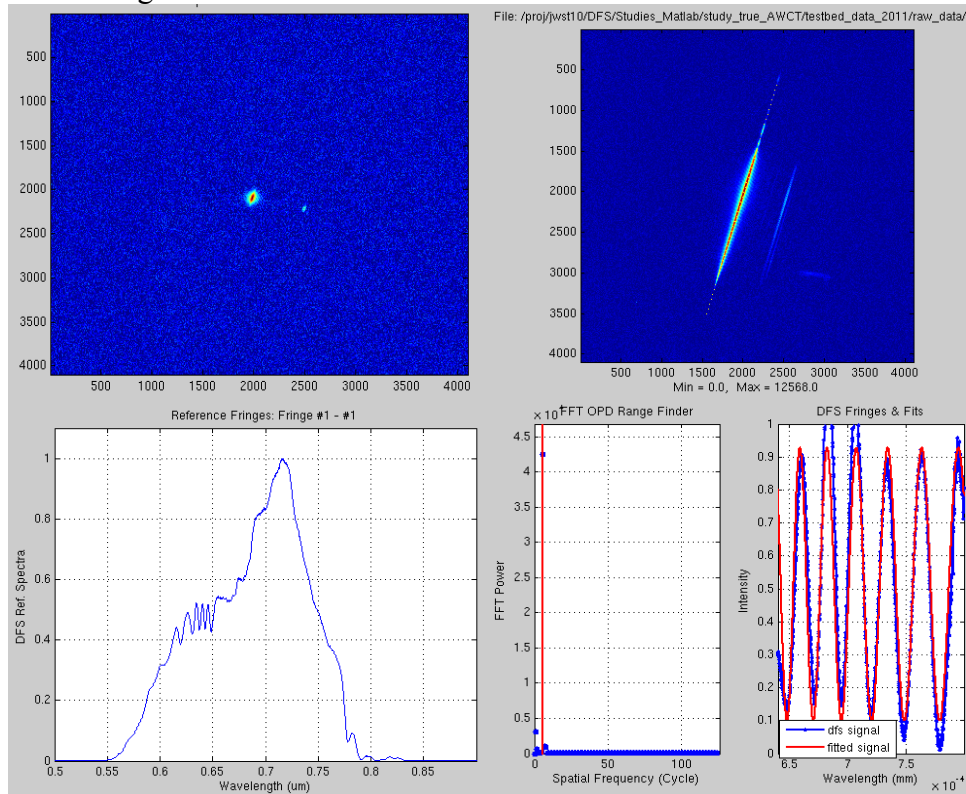


Figure 1 Outline of typical fringe processing

A lot of improvements on previous ADFS algorithm have been implemented over the past year. An end-to-end data analysis tool (written in Matlab) is developed to implement the new ADFS algorithm and has been tested extensively to validate its accuracy and robustness with both the simulated fringe data and the AWCT measurement data. In this section, two major improvements

of the new ADFS algorithm are presented: the expansion of the effective working zone and the multi-dimensional scan scheme.

## 2.2 Expanding the effective working range (oscillation zone and trend-line study)

DFS has its effective working range: at smaller piston zone, the number of the interference fringe is limited, which causes the nonlinear least square data fitting less accurate/stable. At larger piston zone, the visibility drops to an unfavorable signal/noise level, resulting in poor precision. The study with the new ADFS algorithm shows, however, the effective working zone could be further expanded with the multi-trace feature and the interpolation technique of the observed trend-line.

First, ADFS offers some improvements on the small piston zone. Figure 2 left portion shows the fitting error (the difference between the expected piston that was used to generate the simulated fringes and the extracted piston from the simulated fringes) comparison between typical DFS (blue dots) and ADFS (red dots). As expected, DFS error is much larger and still shows the oscillation pattern while ADFS error is tiny and relatively smooth across a larger piston range. The typical DFS/ADFS relies on the single fringe extraction line (FEL) and wavelength calibrations to extract piston information. Applying multi-trace (multiple FEL) and with its averaging effects, the commonly observed oscillation pattern (at small piston zone) can be smoothed out further. Figure 2 right portion shows the oscillation reduction with multi-traces.

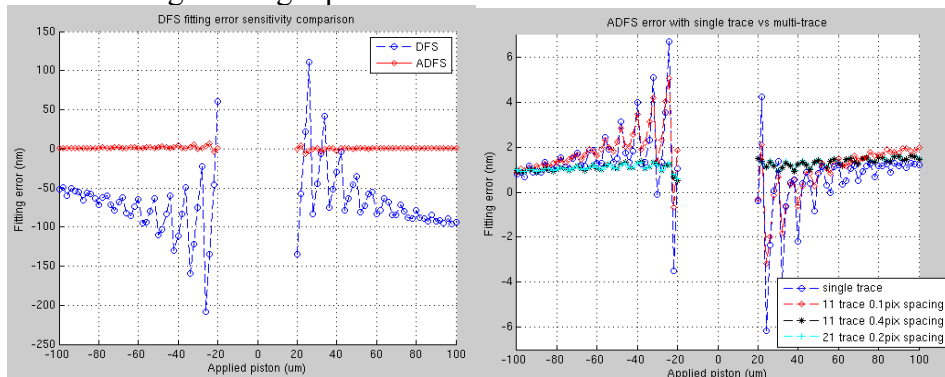


Figure 2 Fitting error comparison (Left: DFS vs. ADFS; Right: single trace vs. multi-trace)

Figure 3 illustrates another interesting observation: a linear slope trend-line existed on the plot of piston error vs. piston. It applies to the whole piston zone (oscillation zone as well)

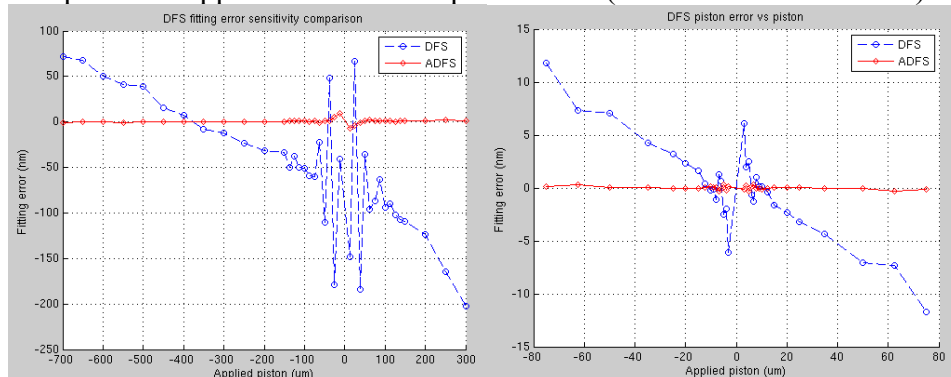


Figure 3 Slope trend line illustration with JWST (left) and AWCT(right)

Further studies shows that the trend line can be explained by the centroid-shifting scheme which is caused by the PSF broaden and overlapping issue due to the diffraction at different wavelengths. In other words, for each wavelength, the crosstalk/contamination (signal from the neighboring channels or wavelengths) causes the centroid at this wavelength shifting around depending on many factors, such as PSF size, grism strength, and source profiles. Extensive study on this trend line had been done and a system metric, called normalized PSF, was proposed to evaluate or benchmark the performance for different DFS systems, a quite useful feature during the designing phase of the DFS system.

The metric formula is defined as  $PSF\_size/(grism\_strength*spectral\_range)$ . For example, JWST DFS system baseline features a grism strength of 1nm/pixel, spectral range of 800nm, and PSF size of 20 pixels, hence its DFS system metric is  $20/(1*800)=0.025$ ; while AWCT DFS baseline system metric is  $30/(1/0.13*400)=0.0098$  with effective PSF size of 30pixel, grism strength of 0.13nm/pixel, and spectral range of 400nm. The metric was set up with the convention that better system has smaller metric (smaller trend line slope). So it is expected that AWCT has smaller trend line slope than JWST does (an improving factor of 2.5). From Figure 3, the extracted trend line slope of AWCT is about 0.12nm/um. Compared with the JWST trend line slope (extracted to be 0.24nm/um), a factor of 2 of improvement on the trend line slope is obtained.

The importance of this trend line study is that, once we extract the trend line slope using a few data points (say, at a few large piston locations), the oscillation zone is essentially vanished. We can use this fitted slope to predict the fitting error at any piston (hence we can compensate it accordingly to improve the algorithm accuracy). This greatly expands the DFS effective zone, improves the algorithm's precision, and boosts the robustness of the algorithm. All those enable DFS to have wider applications.

### **2.3 Multiple-dimensional-scan**

One major issue of the old ADFS is the uncertainty of the solution. With larger angle dithering range, multiple solutions are commonly existed and no single criteria can be universally used to identify the unique solution. To address this problem, a new scheme is proposed: rather than only rotate the fringe extraction line angularly, the translation of the fringe extraction line is also implemented. This extra degree of freedom provides additional limitation on solution identification to ensure its uniqueness.

The FEL lateral translation sensitivity was first studied where FEL rotation center is moving along the FEL and corresponding piston error was calculated. It was shown that the error variation was small and in the order of 2nm even with over 100nm spectral shifting along FEL, i.e., it is relatively insensitive along the FEL direction. This finding suggests us to check the impact of direction perpendicular to FEL, meaning to move FEL parallel. For each DFS fringe, multiple parallel lines from the FEL are defined first. For each parallel line, process the fringe to extract estimated piston and save the RMS of curve fitting with the corresponding FEL parallel offset. For each candidate solution, an averaged RMS (so called global RMS) is calculated among these multiple parallel line. Then the solution with minimal global RMS is defined as the final solution for this fringe. Figure 4 shows the selection process of ADFS solution. The simulated fringe was generated with -80um piston. The measured piston at baseline (nominal FEL) has three solutions (red dots) with FEL dithering range of 0.1deg: -80.7um, -80um, and -

79.3 $\mu\text{m}$ . The old ADFS algorithm will compare the RMS of these red dots and suggests the -79.3 $\mu\text{m}$  as the final solution (but it is the wrong one!). For the new ADFS algorithm, multiple pistons/solutions at different FEL parallel lines (0.5pixel step covering +/-2pixel range from the center baseline FEL) are extracted (blue dots). To define the final solution, for each solution cluster (centering at -80.7 $\mu\text{m}$ /-80 $\mu\text{m}$ /-79.3 $\mu\text{m}$ , respectively, and separated by vertical black lines), RMS are averaged. The criterion of minimal average RMS among solution clusters ensures that correct solution of -80 $\mu\text{m}$  is picked as the final solution.

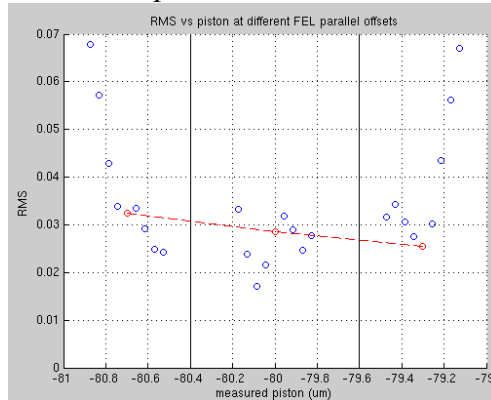


Figure 4 ADFS algorithm solution identification process illustration

Besides the simulated fringe data, the new ADFS algorithm has also been checked and fully tested with the AWCT experimental data taken in 2010. Figure 5 shows the comparison of the old ADFS and the new ADFS algorithm. The improvement of new ADFS happens to be mainly on the case of 4 $\mu\text{m}$  piston (sigma of ADFS is decreased from 400nm to 24nm!) while no difference was found on the 3 $\mu\text{m}$  piston case.

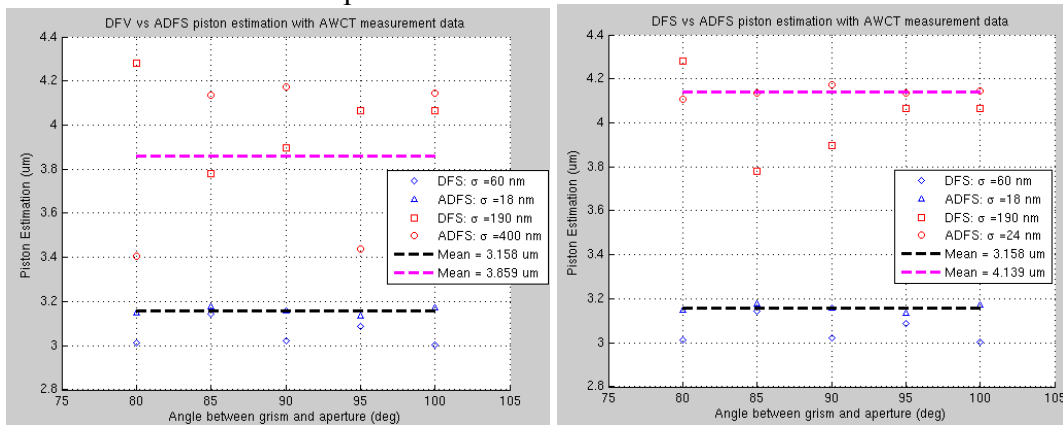


Figure 5 Compare the result of the old ADFS algorithm (left) and the new ADFS algorithm (right) using the AWCT experiment data.

### 3. ADFS SENSITIVITY STUDIES

Like any other physics model, DFS algorithm performance heavily depends on the accuracy of its system parameters. During the development of ADFS, many sensitivity studies on various parameters had been done. This section collects some interesting results of these studies.

### 3.1 baseline model

The AWCT DFS baseline mode has the following parameters: DFs aperture is at diameter of 25mm with separation of 37.5mm. Grism strength is 0.129nm/pixel and the DFS aperture vs. grism angle is set between 70deg to 110deg at step of 10deg to compare the performance at different configurations. The baseline system is a no noise system (aberration free) and has no gravity sag. The spectral range is 500nm to 900nm at center wavelength of 700nm. CCD pixel size is 9 $\mu$ m and resolution is 4096x4096. The system effective focal length is 0.95m, which results in PSF size of  $\sim$ 30pixel. For the baseline study, nominal system parameters are applied without any perturbation. The piston errors (difference between the actual applied piston and the DFS fringe extracted piston) vs. the actual applied piston at different grism/aperture angles are evaluated. Three wavelengths (650nm, 700nm, 850nm) are selected for wavelength calibration where its spot location on CCD is pre-recorded for each wavelength. To extract the fringe line, for each spectral point, grism strength is used to estimate its location on CCD and the so-called “geometric FEL” is formed by connecting those spectral points. Figure 6 shows the piston error & visibility vs. the applied piston for baseline AWCT DFS model at different angles of aperture vs. grism. One observation is that the piston bias (piston error at piston of zero) depends on the angle between the aperture and the grism. Only the case of aperture perpendicular to grism has zero piston bias. Other angles have about -0.35nm/deg sensitivity on piston bias. Secondly, the trend line slope seems to be independent of aperture vs. grism angle. Comparing DFS and ADFS, ADFS has much smaller estimation error and negligible trend line slope. Finally, visibility seems to drop quickly if angle of aperture vs. grism is not at 90deg. To get meaningful and accurate reading, only the data within  $\pm$ 12 $\mu$ m piston (where visibility is  $>$ 0.3) is recommended to use.

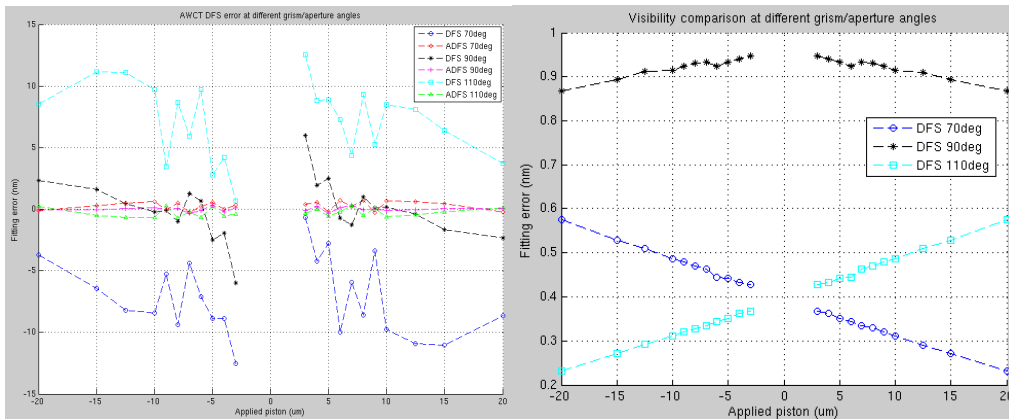


Figure 6 Performance of the AWCT baseline DFS model

### 3.2 FEL sensitivity

To assess the FEL sensitivity, FEL coordinates are perturbed as following: move FEL parallel to its nominal (multi-trace like error); translate FEL along FEL direction (WL reference like error); clock FEL around its center (FEL tilt error). Figure 7 lists the corresponding analysis results. Observations are: 1)for both DFS and ADFS, multi-trace like error is at about 43nm/pix (slightly different in the range of 38nm/pix to 48nm/pix at different angles of aperture vs. grism); 2)for both DFS and ADFS, WL reference like error is at 0.4nm/ $\mu$ m per pix translation along FEL direction; 3)for DFS only, FEL tilt error is about 4nm/mdeg. ADFS is immune to this type of error since its angular rotation search feature self-corrects this kind of clocking error. Further

study shows that these FEL errors/sensitivities are also linear, i.e., if the perturbation is doubled, the piston error is doubled as well to keep the same sensitivity value/rate.

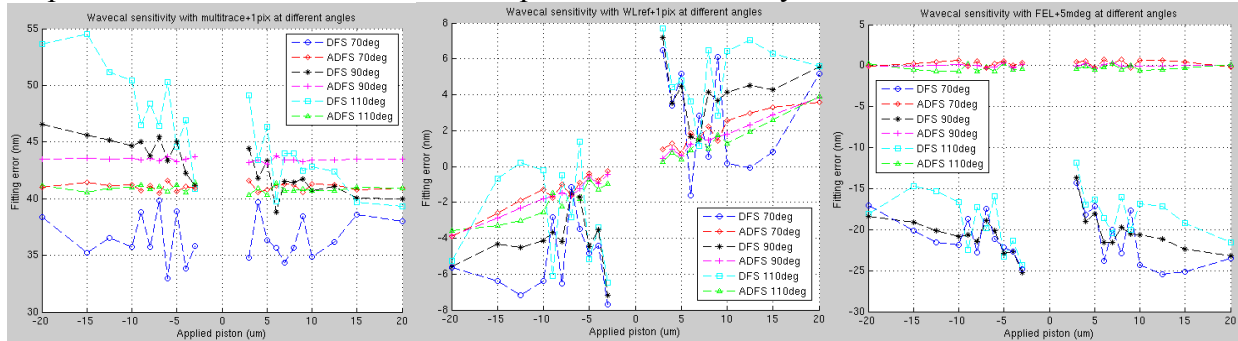


Figure 7 FEL sensitivity: FEL moved along parallel to FEL direction (left); FEL translated along FEL direction (center); FEL clocked around its center (right)

### 3.3 PSF size

As we discussed in Section 2.2, a very important factor on DFS performance is the PSF width/size. A quantitative comparison study was done to see the impact of PSF size. Figure 8 shows the study result with 5 different PSF sizes. As expected, smaller PSF size gets smaller crosstalk between the diffractions at different wavelengths (less overlapping), hence reducing the trend line slope and getting better accuracy across larger piston range. This is consistent with what our previous metric formula (see Section 2.2) predicts: smaller PSF size, better DFS system. Also, larger PSF size drops the visibility much quickly for the same crosstalk reason. The study suggests that small PSF is desirable for the DFS system.

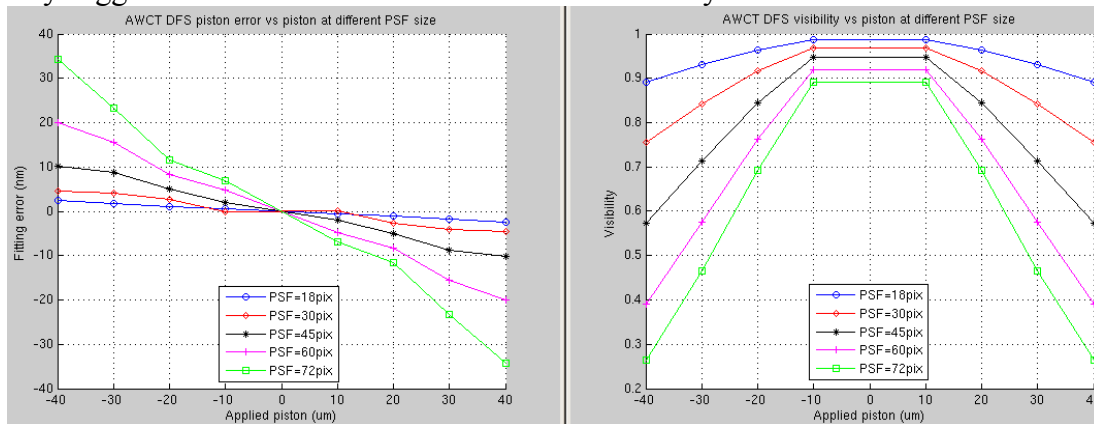


Figure 8 Compare the performance with different PSF size

## 4. Validation of ADFS using AWCT

The newly developed ADFS algorithm has been extensively validated with the AWCT. The section covers the details of this validation process.

### 4.1 AWCT description

Figure 9 shows the optical layout of AWCT in the DFS test configuration. The optical source's wavelength range is 660nm to 780nm (effective range defined by the inserted IR filter in the source). The collimated beam goes through a 4x expander/compressor to reach the DFS aperture

where three mirrors (1 inch diameter) are mounted on actuated stages to form 3 individually controllable segments. The return path beam passes the imaging lens (950mm focal length) and the grism to strike on the camera (9um pixel size and 4096x4096 resolutions). Any combination of two segments, the third segment is tilted away to reduce the crosstalk, will form the interference fringe (DFS fringe) which can be used to extract the relative piston information: the essential idea of the DFS.

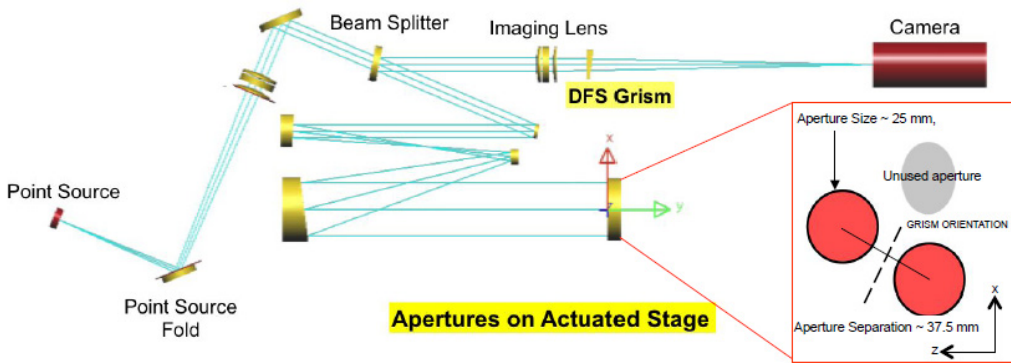


Figure 9 AWCT optical layout in the DFS configuration.

## 4.2 DFS hardware

### 4.2.1 Segments

To simplify the test, current DFS fringe is constructed using only 2 segments while blocking/tilting away the 3<sup>rd</sup> segment. To collect wavelength calibration data, a mechanically driven flipper is also set up for each of these 2 effective segments. Actuated stage for each segment consists of 2 levels of movement: pico motor (coarse mode) and PZT spring gauge (fine mode). The coarse mode is used initially to set 2 segments to generate enough # of fringes (~10-15) for better DFS signal fitting. The fine mode features small range movement (<+/-6um) and is used for DFS test to scan the segment pistons. Before the data collection, segment mounting need to be checked. For example, in the early stage of experiment, some gap/slack between the mirror and the actuator was observed and it affected greatly the repeatability of the collected data. Also, it was found that the centroid of segment drifting vs. time has different patterns (rates) for different segments. To minimize this centroid drifting effect, a good pair of segment needs to be pre-defined/pre-selected. Figure 10 shows the centroid drifting of 3 AWCT segments. With this plot, segment 2/3 pair was selected as the working pair for our experiment.

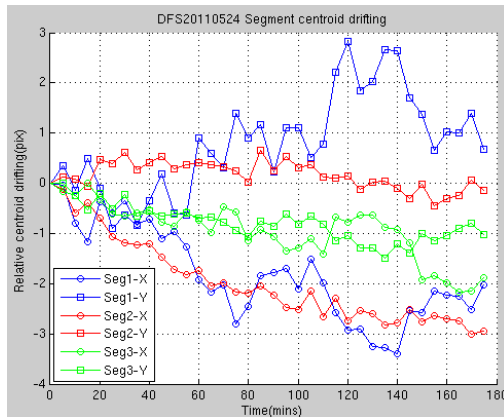


Figure 10 Centroid drifting of three segments

In the lab, it was also noticed that the centroid of the segment is shifting when segment was pistoned to different locations, hinting that the segment is not mounted exactly vertical to the incident beam or pistoning direction. To minimize this misalignment effect, we need to select a good segment to piston while keeping the other one fixed. Figure 11 shows the centroid shifting at different piston locations for the pre-selected seg2/seg3 pair. With this data, segment 3 was defined as the pistoning segment and segment 2 was defined as the fixed segment.

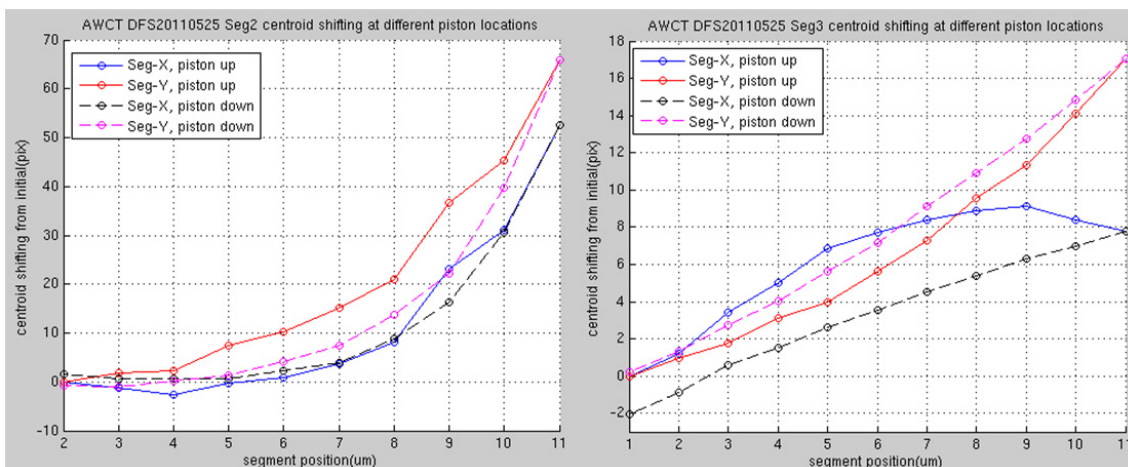


Figure 11 Segment centroid shifting at different piston locations

One final note on segment, it is found that the segment centroid is also varied at different grism angles, and the variation amount is different between segments. The dependence of centroid on grism angle is explainable: different grism rotation has different beam print but only one wavelength can be invariant to the grism rotation. For different segment, beam print is different even with the same grism angle. To maximize the fringe interference, the PSF of these two segments need to be stacked/aligned first. When grism rotates, the previous stacked PSF will be off and centroid difference will be dependent on the grism rotation angles. Figure 12 shows the centroid difference at different grism angles. Obviously, to get optimal performance, the segments need to be restacked at each grism angle. But, current AWCT PSF size is about 30 pixels and variation of a few pixels doesn't affect the performance much (~10%).

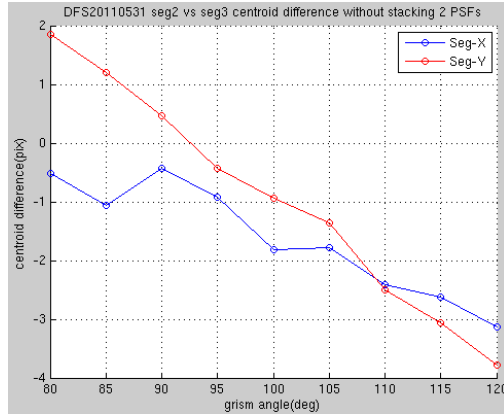


Figure 12 segment centroid difference vs. grism angles

#### 4.2.2 Grism

Grism is another important DFS hardware that needs to be studied carefully to ensure the meaningful data taking successfully. For example, the grism was loosely mounted (glued) in the early stage of the experiment and it caused a lot of uncertainty on data repeatability. Also, depending on the number of wavelength calibration points, the grism strength could be estimated differently. Figure 13 shows different options to extract grism strength. It shows that larger separation and more data points on narrow band filters for wavelength calibration is preferred with smaller variation on grism strength.

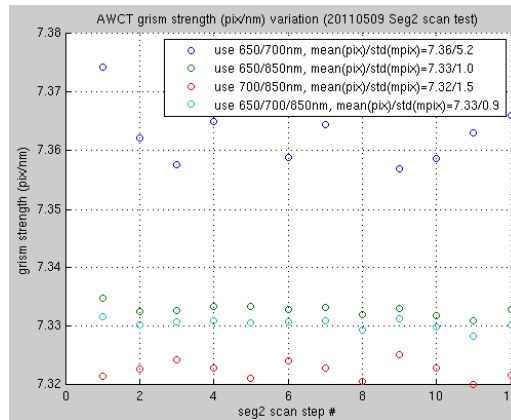


Figure 13 grism strength extracted with different options

#### 4.3 Experiments & data matrix

To process DFS fringe, we need to collect wavelength calibration images and DFS image as the minimal. Wavelength calibration images are taken typically with 3 narrow band filters at 650nm/700nm/850nm while DFS fringe is taken with board band filter. If it is necessary, a dedicated reference image can be taken with single segment at board band filter to extract source profile. Otherwise, the averaged DFS image (center portions along the spectral direction) can be used as the reference image. Due to the camera sensitivity on different spectrums, the exposure time at each image needs to be adjusted accordingly to simultaneously meet the high dynamic range requirement but not saturate the fringe. For example, 850nm narrowband filter needs about 9 second exposure time while 650nm narrow band filter just needs 0.5 second.

Three kinds of experiments are done: piston scan; grism rotation; piston +/-1um step with grism rotation. For piston scan experiment, segment 2 is fixed and segment 3 is scanned roundtrip within a range (+/-5um) at the step of 1um. At each piston location, PSF of two segments are restacked and wavelength calibration images and DFS images are taken. Those images are used to extract piston information, from which the relative movement can be determined and compared against the 1um step to see its accuracy, linearity, and repeatability. For grism rotation experiment, both segments are fixed and grism is clocked from 80deg to 110deg at the step of 5deg. At each grism angle, PSF of two segments are restacked, and wavelength calibration images as well as the DFS images are taken. Those images are used to extract piston information, from which the sensitivity of piston estimation on grism angle could be derived. For piston +/-1um step with grism rotation experiment, first the grism rotation experiment is done at initial piston, then segment 3 is pistoned +1um, and grism rotation experiment is repeated, then segment 3 is pistoned -1um, and the grism rotation experiment is repeated again. This piston scan and grism rotation combination can answer two questions simultaneously: is the 1um mechanical movement really reflecting the 1um from DFS fringe? And, is the piston estimation depending on the grism angle at all?

Table 1 lists the experiment and its data matrix. Data analysis details will be in the next section

experiment name	Date	grism angle	segment range
grism rotation test	5/31	80~110 at step of 5deg	seg2/seg3 = 1um/6um
	6/2	80~120 at step of 5deg	seg2/seg3 = 1um/6um
piston scan at 90deg grism angle	5/25	90	2um-11um-2um
	5/26	90	6um-2um-6um
	5/27	90	6um-2um-6um (4 times)
	5/31	90	6um-2um-6um
	5/31	90	6um-11um-2um-6um
piston scan at different grism angles	5/27	80 & 110	6um-2um-6um
grism rotation +/-1um piston step	5/25	80~110 at step of 5deg	1um-2um-1um;
	5/27	80~110 at step of 5deg	6um-5um-6um

Table 1 List of AWCT DFS validation experiment data

## 4.4 Data analysis

### 4.4.1 grism rotation test

Figure 14 shows the estimated piston from the DFS fringes and the segment centroid difference at different grism rotation angles. The data suggest that there is a correlation between piston estimation and segment centroid with about 55nm/pix for DFS and 22nm/pix for ADFS. Notice that this piston over centroid sensitivity includes the centroid drifting impact as well (Section 4.2.2 demonstrated that the segment centroid drifts differently for different segments).

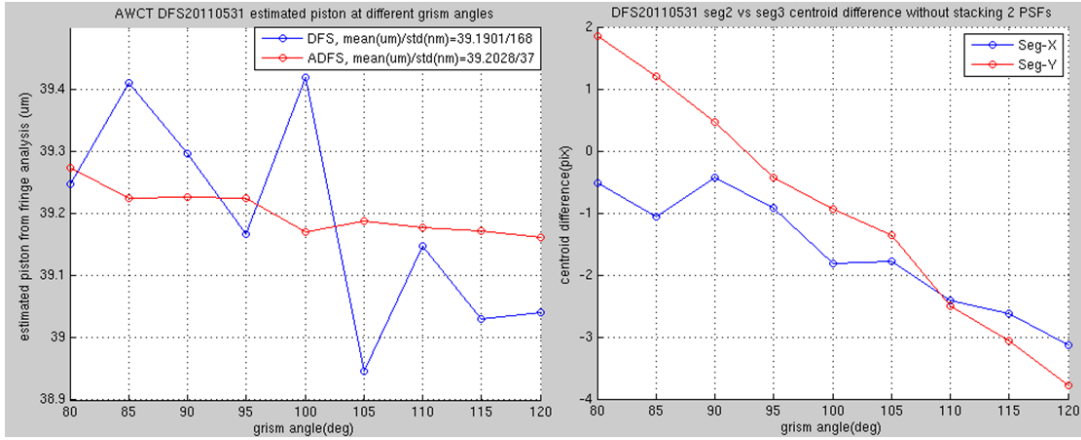


Figure 14 Grism rotation test data analysis results

#### 4.4.2 piston scan test

Segment is driven through PZT spring gauge which has some hysteresis (or inertia) observed. For example, typically about 6V change is needed to piston segment 1um, but about 8V change is needed when changing the piston moving direction. Also, as segment moves, it needs smaller and smaller voltage change to get the same 1um movement, i.e., it is getting the momentum. Detailed study/data taking reveals that the current PZT drive has a linearity of 6.3V/um with standard derivation of 1V (~15% uncertainty in its linearity) and its repeatability (return to the same piston with same voltage) is about 0.86, meaning that it can only return to the same location with +/-14% margin.

Figure 15 shows the piston scan test data taken on different dates and with different scan range/sequence. Overall, it extracts ~0.9um from the DFS fringes for a 1um piston movement. Comparing with DFS, ADFS is much more stable with much smaller standard derivation.

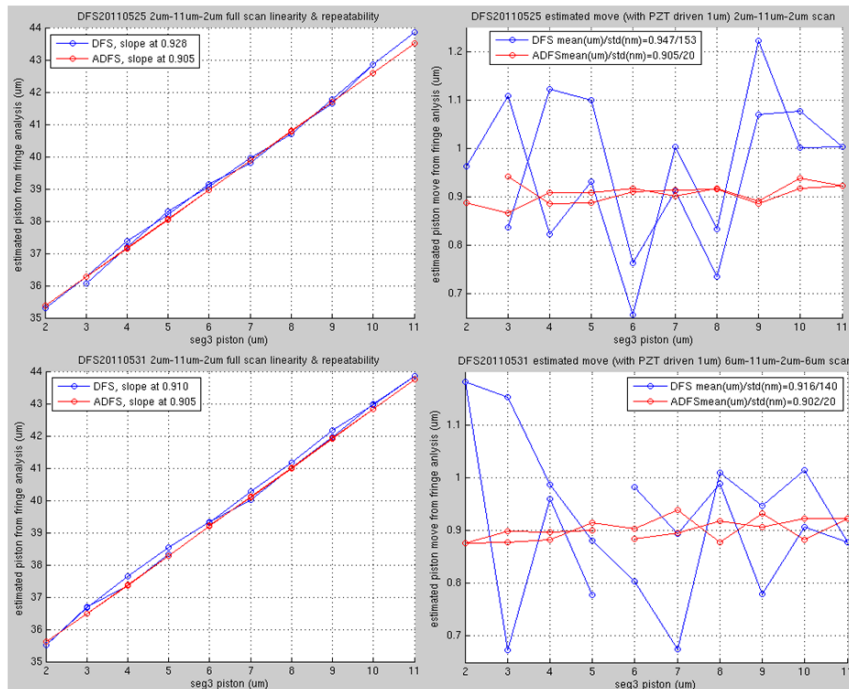


Figure 15 piston scan test data analysis results

To further validate the data, both the repeatability check on the piston scan and the sensitivity check on the grism angle were carried out. Figure 16 shows the results for these two checks. Once again, compared with DFS performance, ADFS has much smaller variation on piston repeatability and is much less sensitive on grism angle.

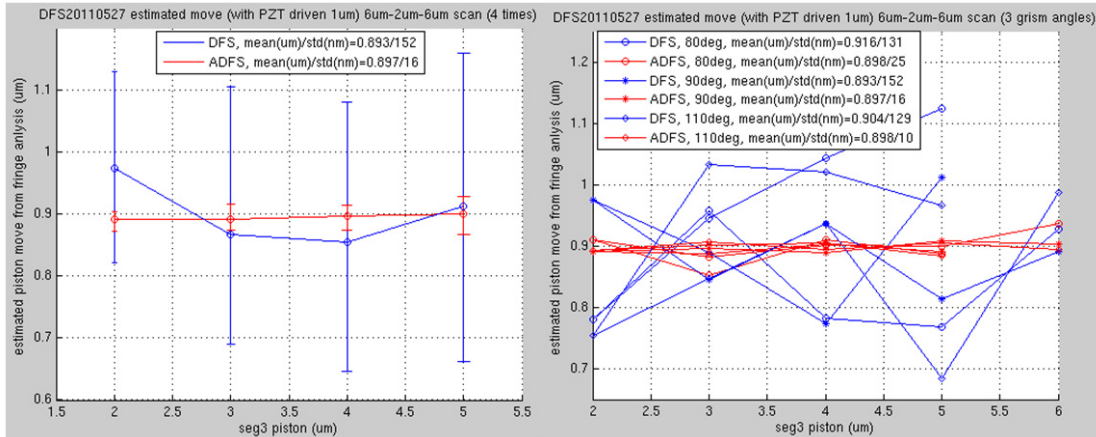


Figure 16 piston scan test with repeatability check and grism angle sensitivity check.

#### 4.4.3 Grism rotation +/-1um piston step test

For this test, we will take grism rotation data at starting location, repeat the data taking at +1um location and at the (back to) starting location. Figure 17 shows the data result which again demonstrates that the variation of ADFS algorithm is much smaller than that of DFS. The up or down scan has about the same piston mean and variation.

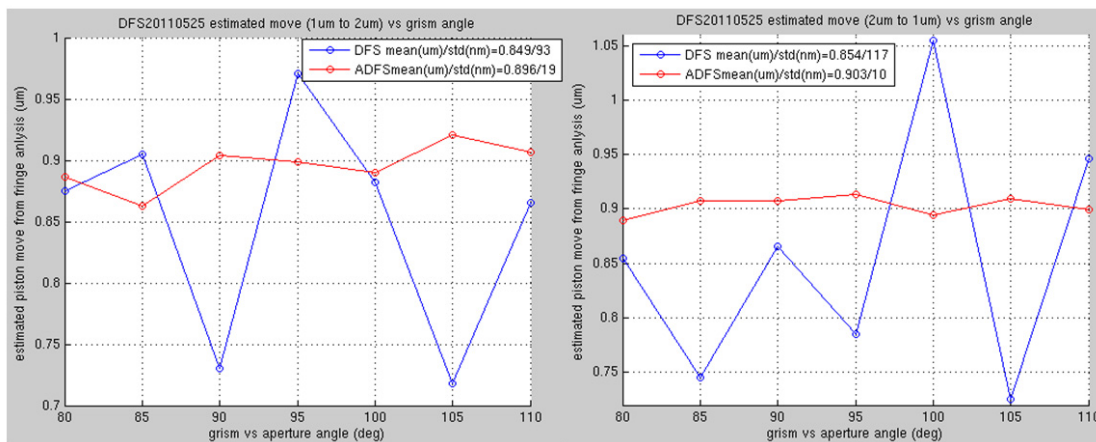


Figure 17 Grism rotation +/-1um piston step results: up scan (left) and down scan (right)

#### 4.4.4 Data analysis summary

Table 2 lists the data analysis summary from AWCT DFS experiment data. It clearly shows that although the absolute piston difference between DFS and ADFS is small, but the variation of ADFS is much smaller than that of DFS, i.e., ADFS algorithm is far more stable/robust than DFS algorithm.

experiment name	Date	DFS mean(um)	ADFS mean(um)	DFS std(nm)	ADFS std(nm)
grism rotation test	5/31	39.190	39.203	168	37
	6/2	39.229	39.191	151	38
piston scan at 90deg grism angle	5/25	0.947	0.905	153	20
	5/26	0.894	0.890	158	16
	5/27	0.893	0.896	152	16
	5/31	0.891	0.897	45	11
	5/31	0.916	0.902	140	20
piston scan at different grism angles	5/27	0.910	0.898	130	16
grism rotation +/-1um piston step	5/25	0.852	0.899	105	14
	5/27	0.921	0.913	34	22

Table 2 AWCT DFS data analysis summary

Figure 18 summarizes all data of 1um piston scan done at different date, different scan range, and difference experiment type to just get some statistics. The distribution/histogram also shows clearly the advantage of ADFS over DFS on the algorithm stability.

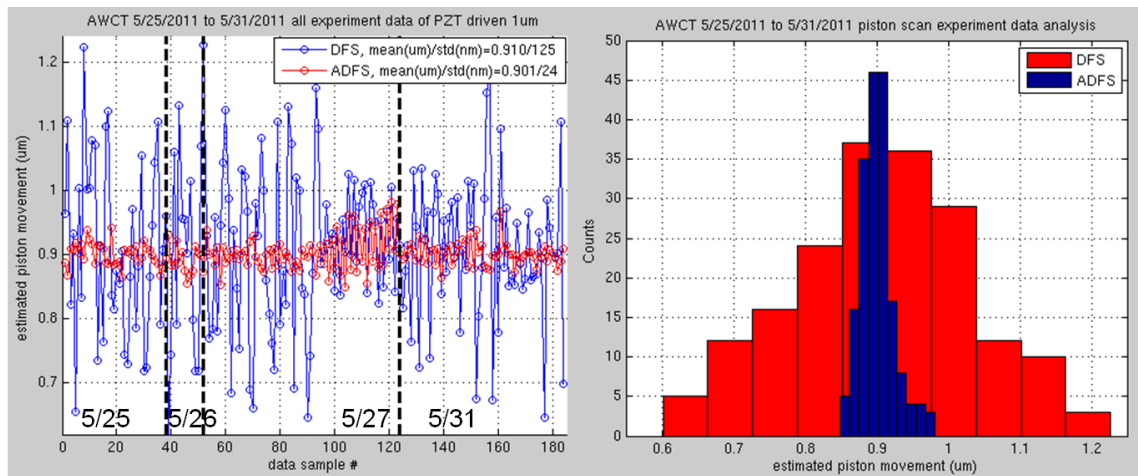


Figure 18 1um piston scan experiment data assembly/distribution

#### 4.5 Piston reference (1um) validation using Range-Gate-Metrology (RGM)

As we can see from previous section that 1um mechanical movement seems not to be exactly the 1um from DFS fringe extraction (~10% difference observed). Since the PZT driving gauge used in the experiment has been used for a few years without calibration, we checked/calibrated the 1um movement using a custom made Range-Gated-Metrology (RGM) system<sup>4</sup>. Figure 19 is the testing setup: beam launcher and corner cube (left side of the figure) are mounted in the same platform about 1m away from segments (right side of the figure). A paper tube is used in between to reduce the air turbulence. The measurement beam double passes segment mirror which is tilted by picomotors to maximize the RMS signal strength. Segment actuator driver is commanded via RS232 from the laptop running Matlab script. Data is captured by freezing and saving the RGM live display figure from Matlab.

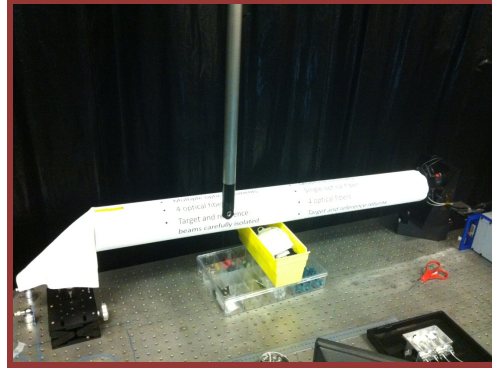


Figure 19 Segment RGM calibration setup

For data analysis, the OPD/amplitude data was extracted from the saved Matlab figure fields (each figure plot contains about 2500 data points over 10 sec). Threshold is applied manually to select the “upper” and “lower” flat portion of the signals (see the red and green sections in Figure 20). Each portion is then averaged to provide one OPD measurement. The final delta OPD from RGM is calculated from the difference between all the mean upper OPD and all the mean lower OPD. For example, with the specific data set shown in Figure 20, RGM OPD difference is 3580nm while the expected segment movement is 4000nm, hence we calibrated  $1\mu\text{m}$  mechanical piston movement into  $3580/4000 = 0.895\mu\text{m}$ . This compares with our fringe measurement extraction of  $0.9\mu\text{m}$  using ADFS algorithm.

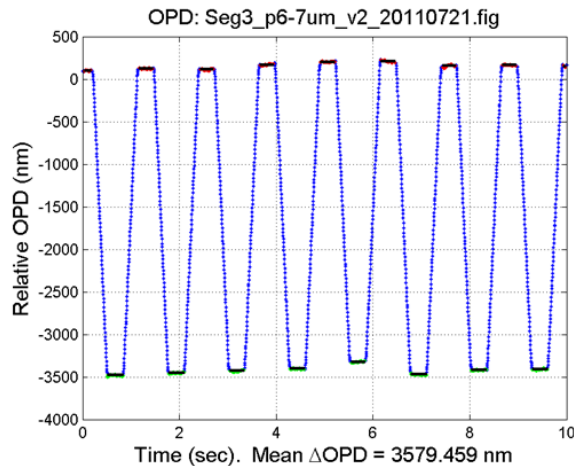


Figure 20 Segment RGM data. Blue dots: raw data; red dots: threshold selected upper portion; green dots: threshold selected lower portion; thick black lines: mean OPD for that portion

For completeness, we calibrated all 3 segments at different piston ranges using RGM system. Table 3 lists the full calibration results. Two observations can be drawn from this table: 1) Segment #2’s RGM measurement is larger than the expected OPD while for the segment #3 it is the opposite. 2) For all segments the RGM measured OPD increases as the segment piston moving toward the upper range.

Segment Number	Expected OPD from PZT command	Lower Range Piston Measured (2 – 3 $\mu\text{m}$ )	Middle Range Piston Measured (6 – 7 $\mu\text{m}$ )	Upper Range Piston Measured (9 – 10 $\mu\text{m}$ )	Average calibrated 1 $\mu\text{m}$ piston
1	4000 nm	3973.157 nm	4057.745 nm	4110.610 nm	<b>1.012 <math>\mu\text{m}</math></b>
2	4000 nm	4129.779 nm	4168.219 nm	4256.722 nm	<b>1.046 <math>\mu\text{m}</math></b>
3	4000 nm	3544.534 nm	3579.459 nm	3614.939 nm	<b>0.895 <math>\mu\text{m}</math></b>

Table 3 Three segment RGM calibration results

For the first observation, interestingly, we did have some piston scan data taken with Segment 2 as the moving segment in the early stage of this algorithm validation process. Figure 21 shows one example of data taken with Segment 2 as the piston segment. Comparing with what we got from RGM calibration, the agreement is quite well (1.041 $\mu\text{m}$  of fringe extraction vs. 1.046 $\mu\text{m}$  of RGM calibration). Combined with the comparison on Segment 3 (0.901 $\mu\text{m}$  of fringe extraction vs. 0.895 $\mu\text{m}$  of RGM calibration), this excellent agreement (<6nm or <1%) on different segment responses to the same 1 $\mu\text{m}$  PZT movement between fringe extraction through ADFS algorithm and the RGM calibration result further validates the effectiveness and robustness of the new ADFS algorithm. The different response among different segments also suggests that segments are due for the recalibration (last calibration was ~4 years ago).

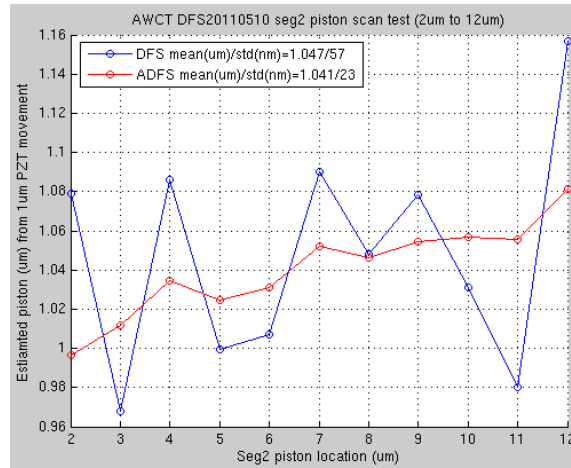


Figure 21 Segment 2 piston scan test results

For the second observation which is also nicely confirmed by the piston scan data in Figure 15, 16, and 21, it suggests that the spring gauge behave slightly nonlinearly when it does piston scans, i.e., it could accumulate some momentums after initial movement. This is consistent with what we observed on the PZT voltage for driving 1 $\mu\text{m}$  mechanical movement: smaller voltage is needed at upper range of piston.

## 5. Conclusion

A high precision, effective, and robust ADFS algorithm has been successfully developed. The new ADFS algorithm greatly expands the DFS effective working zone into the previously

unusable region. The multiple-dimensional-scan scheme, combined with the global minimal RMS criterion, ensures the unique and accurate solution. The algorithm has been thoroughly tested with many sensitivity studies on various well-thought noises and perturbations with simulated fringes. Finally the algorithm has been extensively validated through AWCT measurement data.

### **ACKNOWLEDGEMENT**

This research was carried out at the Jet Propulsion Laboratory, California Institute of Technology, under contract with the National Aeronautics and Space Administration (NASA). The funding is coming from the Retention Investment Projects with the Project number of PEIN07 and Task Number of 35.38.1.01. Some of the simulation study presented in this report is funded by the JWST project 104020.01.01.

### **REFERENCES**

- [1] F. Shi, D. C. Redding, C. W. Bowers, A. E. Lowman, S. A. Basinger, T. A. Norton, P. Petrone III, P. S. Davila, M. E. Wilson, and R. A. Boucarut, "DCATT dispersed fringe sensor: modeling and experimenting with the transmissive phase plates," Proc. SPIE 4013, 757-762 (2000)
- [2] J. A. Spechler, D. J. Hoppe, N. Sigrist, F. Shi, B. Seo, and S. Bikkannavar, "Advanced DFS: A Dispersed Fringe Sensing Algorithm Insensitive to Small Calibration Errors", Proc. SPIE, 7731(55), (2010)
- [3] F. Shi, S.A. Basinger, R. T. Diaz, R. O. Gappinger, H. Tang, R. K. Lam, E. Sidick, R. C. Hein, M. Rud, and M. Troy, "Advanced wavefront sensing and control testbed (AWCT)", Proc. SPIE, 7739(2), (2010)
- [4] Oliver Lay, "Range Gated Metrology", AMD Doc-share#398953, (2008)